Brain Topogr
DOI 10.1007/s10548-008-0056-3

ORIGINAL PAPER

Integrated MEG/fMRI Model Validated Using Real Auditory Data

Abbas Babajani-Feremi · Hamid Soltanian-Zadeh · John E. Moran

Accepted: 20 April 2008

Abstract The main objective of this paper is to present methods and results for the estimation of parameters of our proposed integrated magnetoencephalography (MEG) and functional magnetic resonance imaging (fMRI) model. We use real auditory MEG and fMRI datasets from 7 normal subjects to estimate the parameters of the model. The MEG and fMRI data were acquired at different times, but the stimulus profile was the same for both techniques. We use independent component analysis (ICA) to extract activation-related signal from the MEG data. The stimulus-correlated ICA component is used to estimate MEG parameters of the model. The temporal and spatial information of the fMRI datasets are used to estimate fMRI parameters of the model. The estimated parameters have reasonable means and standard deviations for all subjects. Goodness of fit of the real data to our model shows the possibility of using the proposed model to simulate realistic datasets for evaluation of integrated MEG/fMRI analysis methods.

Keywords Electroencephalography (EEG) · Magnetoencephalography (MEG) · functional magnetic resonance imaging (fMRI) · Integrated modeling · Independent component analysis (ICA)

A. Babajani-Feremi (✉) · H. Soltanian-Zadeh
Image Analysis Laboratory, Radiology Department, Henry Ford Hospital, One Ford Place, 2F, Detroit, MI 48202, USA
e-mail: abbasb@rad.hfh.edu

H. Soltanian-Zadeh
Control and Intelligent Processing Center of Excellence, Electrical and Computer Engineering Department, University of Tehran, Tehran 14395-515, Iran

J. E. Moran
Neuromagnetism Laboratory, Neurology Department, Henry Ford Hospital, Detroit, MI 48202, USA

Introduction

Magnetoencephalography (MEG) and functional magnetic resonance imaging (fMRI) have complementary spatial and temporal resolutions. fMRI has good spatial resolution, but poor temporal resolution due to the limited rate of change in the hemodynamic response. On the other hand, MEG has good temporal resolution, but its spatial resolution is poor due to the inverse problem being ill-posed (Hämäläinen et al. 1993). Integrated MEG/fMRI analysis should improve the overall spatiotemporal resolution of the results based on the fact that MEG and fMRI are different views of a common source (neural activity) (Dale and Halgeren 2001; Dale et al. 2000; Horwitz and Poeppel 2002; Korvenoja et al. 2001; Liu et al. 1998, 2006; Martinez-Montes et al. 2004).

Although MEG and fMRI signals originate from common sources (neural activities), there may be differences between the spatiotemporal responses of the two techniques (Nunez and Silberstein 2000). An integrated bottom-up model based on physiological principles can illustrate the relationship between MEG and fMRI. However, there are limited works about MEG, electroencephalography (EEG), and fMRI integrated modeling in the literature (Babajani et al. 2005; Babajani and Soltanian-Zadeh 2006; Daunizeau et al. 2007; Riera et al. 2005, 2006, 2007).

In the integrated model proposed in (Riera et al. 2005), a two-dimensional autoregressive model with exogenous variables (ARx) was introduced to describe the relationships between synaptic activity and hemodynamic responses. A static nonlinear function was used to describe

the electro-vascular coupling through a flow-inducing signal. Their assumption about a linear relationship between cerebral blood flow (CBF) and the Blood Oxygen Level Dependent (BOLD) signal is not generally valid (Buxton et al. 1998), which they corrected (Riera et al. 2006) using the extended Balloon model (EBM) (Friston et al. 2000).

We proposed an integrated MEG/fMRI model (Babajani et al. 2005) where post-synaptic potentials (PSPs) were the main link between MEG and fMRI (Fig. 1). For a given external stimulus in this model, a linear model represented the number of active PSPs at each point in time. Several parameters of PSPs were introduced and modeled using random variables. Different aspects of PSPs were considered for constructing the MEG and fMRI signals from the overall synaptic activities. The MEG signal was constructed using the resultant overall synaptic activities and solution of the forward problem. The fMRI signal was constructed using the resultant overall synaptic activities as the input of the EBM. Using simulation studies, we showed that the parameters of the model can explain conditions for which there is a detectable fMRI signal in an area while this area may be silent for MEG and vice versa.

Based on our proposed extended neural mass model, we introduced another integrated model of MEG/EEG and fMRI signals based on the physiological principles of the cortical minicolumns and their connections (Babajani and Soltanian-Zadeh 2006). In this model, MEG signals are generated by synaptic activations of the pyramidal cells and subsequent currents in minicolumns. By introducing a relationship between the stimulus and the overall neural activity and using it as the input of the EBM, we extracted the fMRI signal from the proposed extended neural mass model. We validated the proposed model by comparing the simulation results with the experimental results.

The main aim of the current paper is to determine the parameters of our proposed model (Babajani et al. 2005) using real MEG and fMRI datasets. While it was impossible to record MEG and fMRI signals simultaneously, these data were gathered from 7 normal subjects using the same auditory stimulus as shown in Fig. 2. After calculating the average MEG block response, we used independent component analysis (ICA) to extract the MEG signal of the brain activity occurring in the primary auditory cortex. This signal was used to estimate parameters of the linear filter in Block 1 of Fig. 1. The corresponding spatio-temporal sequence of the fMRI activation, measured in the primary auditory cortex, was used to estimate the fMRI parameters of the proposed model. The proposed model with estimated values of its parameters can be used to simulate realistic datasets for evaluation of the integrated MEG/fMRI analysis methods.

The organization of the paper is as follows. The summary of the proposed model in (Babajani et al. 2005), description of the real auditory datasets, and estimation of the parameters of the proposed model are presented in next section followed by Discussion and Conclusions.

Estimation of the Model Parameters

Our proposed integrated MEG/fMRI model (Babajani et al. 2005) is shown in Fig. 1. For a given external stimulus, $N(t)$ is the number of active post synaptic potentials (PSPs) in the corresponding active cortical area and is calculated using a linear temporal filter. The overall generated dipoles in the area can be calculated using the following equation:

$$\bar{Q}(t) = K_M \cdot N(t) \tag{1}$$

where K_M is a fixed stimulus-related parameter and $\bar{Q}(t)$ is the overall generated dipoles in the active cortical area. The generated MEG signal is calculated using Eq. 1 and the solution of the forward problem as follows:

$$B(t) = G\,\bar{Q}(t) \tag{2}$$

where G is the lead field matrix and $B(t)$ is the measured field by the MEG sensors (Baillet et al. 2001). For the forward solution, we utilize a spherical head model with the sphere center calculated for six separate skull regions (left and right anterior, left and right central, and left and right posterior). For each local sphere, the radius and

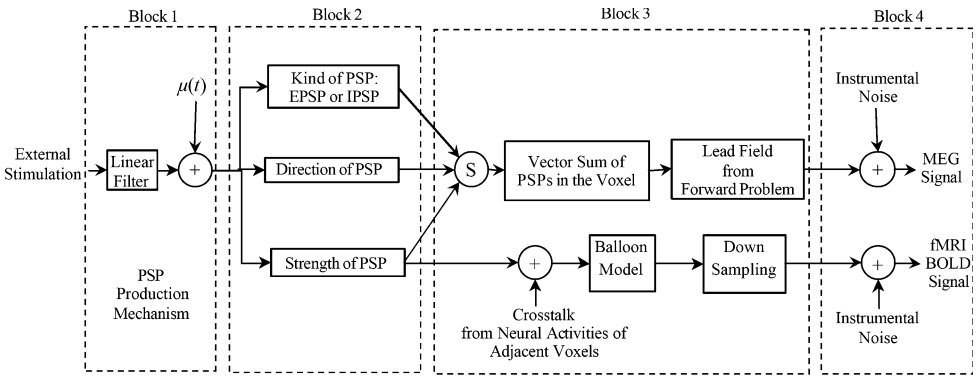

Fig. 1 Schematic diagram of the proposed integrated MEG and fMRI model (Babajani et al. 2005)

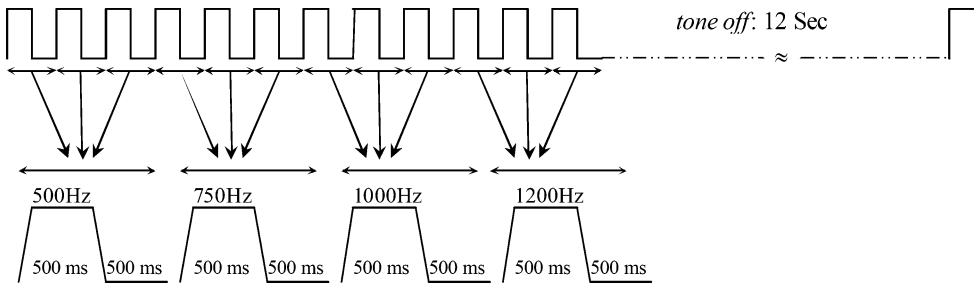

Fig. 2 Illustration of one epoch (block) of the stimulus profile for an auditory excitation. Each epoch contains 12 s of *tones on* and 12 s of *tones off*. During the *tones on* period, 3 tone bursts were presented with a 15 ms rise/fall time at a rate of one per second for each of 4 tone frequencies 500, 750, 1,000, and 1,200 Hz. MEG data of all subjects contained 50 epochs, but the number of fMRI blocks was different for different subjects (see Table 1)

sphere center were determined by performing a least square fit of the sphere to the local skull surface digitization points (Moran et al. 2001).

Referring to Eqs. 19 and 21 in (Babajani et al. 2005), the overall synaptic activities due to the external stimulus can be calculated as follows:

$$\begin{cases} \bar{u}(t) = K_f \cdot N(t) \\ K_f = \frac{u_m}{\max(N)} \end{cases} \tag{3}$$

where $\bar{u}$ is the overall synaptic activities in the active cortical area, u_m is the synaptic activity that produces the maximum output in the extended Balloon model, max(N) shows the maximum number of the active PSPs in the active area, and $N(t)$ represents the number of active PSPs. The calculated overall synaptic activity in (3) was used as the input of the EBM with the following equations:

$$\begin{cases} \ddot{f} = \varepsilon \bar{u}(t) - \dot{f}/\tau_s - (f-1)/\tau_f \\ \dot{v} = \frac{1}{\tau_0}(f - v^{1/\alpha}) \\ \dot{q} = \frac{1}{\tau_0}\left(f\frac{1-(1-E_0)^{\frac{1}{f}}}{E_0} - qv^{\frac{1}{\alpha}-1}\right) \\ y(t) = V_0(k_1(1-q) + k_2(1-q/v) + k_3(1-v)) \end{cases} \tag{4}$$

where the blood flow f, the blood venous volume v, and the veins deoxyhemoglobin content q are three state variables normalized to their rest values and y is the BOLD output signal. The neural efficiency (ε), the signal decay (τ_s), the autoregulation (τ_f), the venous transit time (τ_0), the stiffness (α), the oxygen extraction at rest (E_0), and the resting blood volume fraction (V_0) are the physiological parameters of the EBM. For a 1.5 T scanner and TE = 40 ms, parameters k_1, k_2, and k_3 have been evaluated to be $k_1 = 7E_0$, $k_2 = 2$, and $k_3 = 2E_0$-0.2 in (Buxton et al. 1998).

Auditory Task Data

We need real MEG/fMRI datasets to estimate the parameters of the model. Some parameters of the model like K_M in (1) are dependent on the kind of stimulus. For example, we expect different spatial responses (different K_M) for visual and auditory stimuli. In this study, we estimate the parameters of the model using the auditory stimulus shown in Fig. 2. However, the procedure for estimating the parameters of the model is the same for other types of stimuli. One block of the auditory on/off stimulus is shown in Fig. 2. The first 12 s consist of *"tones on"* followed by 12 s of "*tones off.*" During the *"tones on"* period, half second tone bursts with a 15 ms rise/fall time are presented at a rate of one per second. Three tone bursts are presented sequentially for each of 4 tone frequencies in the following order: 500, 750, 1,000, and 1,200 Hz. While it is impossible to gather MEG and fMRI data simultaneously, this auditory block stimulus is used for both MEG and fMRI studies of 7 healthy subjects (4 males and 3 females, from 27 to 44 years old). In addition, 3-D anatomical MRI data is used for co-registering fMRI and MEG coordinates. Specifications of the acquired MRI and fMRI data from the subjects are given in Table 1.

For the fMRI data, we used a 1.5 T GE scanner and the echo planner imaging (EPI) sequence with 64 by 64 data acquisition matrix (see Table 1 for details). Auditory stimuli are presented through air conductance tubes to headphones to reduce external noise. We utilized the air tubes just for gathering the fMRI datasets. The phase delay due to sound propagation in the tube is on the order of 10 ms considering 3–4 m length of the tubes and 345 m/s speed of sound. This delay is negligible in the case of the fMRI signal. The MEG data is gathered by a 148-channel whole head Neuromagnetometer (4D Neuroimaging). Measurements are taken inside a magnetically shielded room located in the Neuromagnetism Laboratory of Henry Ford Hospital (HFH), Detroit, Michigan, USA. Fifty blocks (epochs) of the MEG data are acquired for all subjects, sampled at 508.63 Hz, and initially band-pass filtered between 0.1 and 100 Hz before disk storage.

Preprocessing

We use statistical parametric mapping (SPM) for activation detection of the fMRI data. After discarding the first few

Table 1 Specification of the MRI and fMRI datasets used for estimating the parameters of the proposed model

Subject #	Gender	Age	MRI		fMRI					
			Resolution	Voxel size (mm^3)	Resolution	Voxel size (mm^3)	Volume Number	TR (s)	TE (ms)	Number of stimulus block
1	Female	44	256 × 256 × 60	0.94 × 0.94 × 2.5	64 × 64 × 14	3.75 × 3.75 × 5.0	132	3	40	16.5
2	Female	40	256 × 256 × 60	0.94 × 0.94 × 2.5	64 × 64 × 16	3.75 × 3.75 × 5.0	198	2	30	16.5
3	Male	33	256 × 256 × 66	0.94 × 0.94 × 2.5	64 × 64 × 16	3.75 × 3.75 × 5.0	198	2	30	16.5
4[a]	Female	41	256 × 256 × 62	0.94 × 0.94 × 2.5	64 × 64 × 14	3.75 × 3.75 × 5.0	198	2	30	16.5
5[a]	Male	33	256 × 256 × 64	0.94 × 0.94 × 2.5	64 × 64 × 16	3.75 × 3.75 × 5.0	198	2	30	16.5
6	Male	27	256 × 256 × 154	0.94 × 0.94 × 1.0	64 × 64 × 34	3.75 × 3.75 × 3.5	120	2	30	10
7	Male	35	256 × 256 × 154	0.94 × 0.94 × 1.0	64 × 64 × 34	3.75 × 3.75 × 3.5	120	2	30	10

[a] Two fMRI datasets are acquired

volumes, we performed realignment and co-registration using SPM5. For finding the active voxels, the stimulus is convolved with three basis functions (HRF, HRF time derivative and HRF dispersion). A cluster of voxels above a statistical threshold is selected for each subject, focusing on the left and right primary auditory cortices. For each of the active voxels, the average BOLD signal over all blocks is calculated after removing DC offset and linear trend. In the next section, we use this average BOLD signal to estimate fMRI parameters in these voxels for all subjects. The detected activation of a representative subject co-registered to MRI is shown in Fig. 3.

We use MEG-Tools (http://www.megimaging.com/) for co-registration of the MEG data with the 3-D anatomical MRI data. The MEG localizations are computed with reference to the Cartesian coordinate system defined by a set

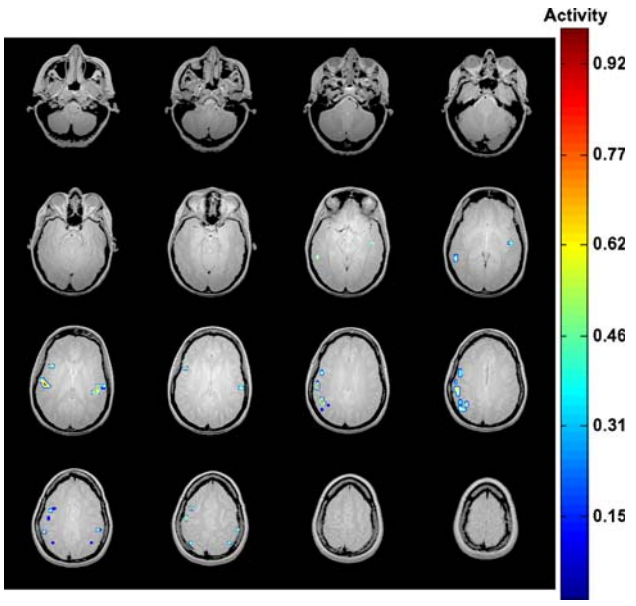

Fig. 3 Illustration of the detected activation from the fMRI data of subject #2 co-registered to 3-D anatomical MRI data after removing single active voxels

of three anatomical landmarks (fiducial points): the right and left external meatus or pre-aurical and nasion. Prior to the MEG scan, the head surface is digitized using laser fast track scanning. The head digitization points (about 3,000 points) are used to ensure a precise registration, when the points laid on the scalp surface of the MRI scan.

The MEG data were band-pass filtered 0.5–30 Hz before analysis. For each subject, 50 epochs of MEG data were recorded. The duration of each epoch is 24 s, similar to the stimulus profile shown in Fig. 2. Bad epochs (blocks) containing eye blinks were discarded, and the remaining epochs averaged to obtain the MEG signal time-locked to tone presentations with a sufficient signal to noise ratio (SNR) for this study. As shown in Fig. 4, we did not extract unique MEG signals for each separate tone frequency as required for imaging the tonotopic organization of the auditory cortex, where locations of responses in the auditory cortex for these tone frequencies vary systematically with frequency by approximately 5 mm or less (Talavage et al. 2004). Rather, after discarding malfunctioning channels, we performed ICA signal separation to extract the most significant signal from the primary auditory cortex that was common to all tone frequencies. In addition, ICA was used to extract heart artifact from the data. Both "Fast-ICA" and AMUSE (Algorithm for Multiple Unknown Source Extraction) (Tong et al. 1991) algorithms were evaluated for extracting MEG signals from the primary auditory cortex from these MEG datasets. We obtained a higher SNR from AMUSE compared to "Fast- ICA", confirming superiority of AMUSE for abstracting long duration signals with significant autocorrelations over time, as reported in (Moran et al. 2004). Therefore, AMUSE was used to extract MEG signals from the primary auditory cortex of all subjects.

The ICA components generated by applying AMUSE to the MEG data were sorted according to the amount they contributed to the time-correlated signal power of the AMUSE algorithm. The three most powerful components of the MEG data of a representative subject are illustrated

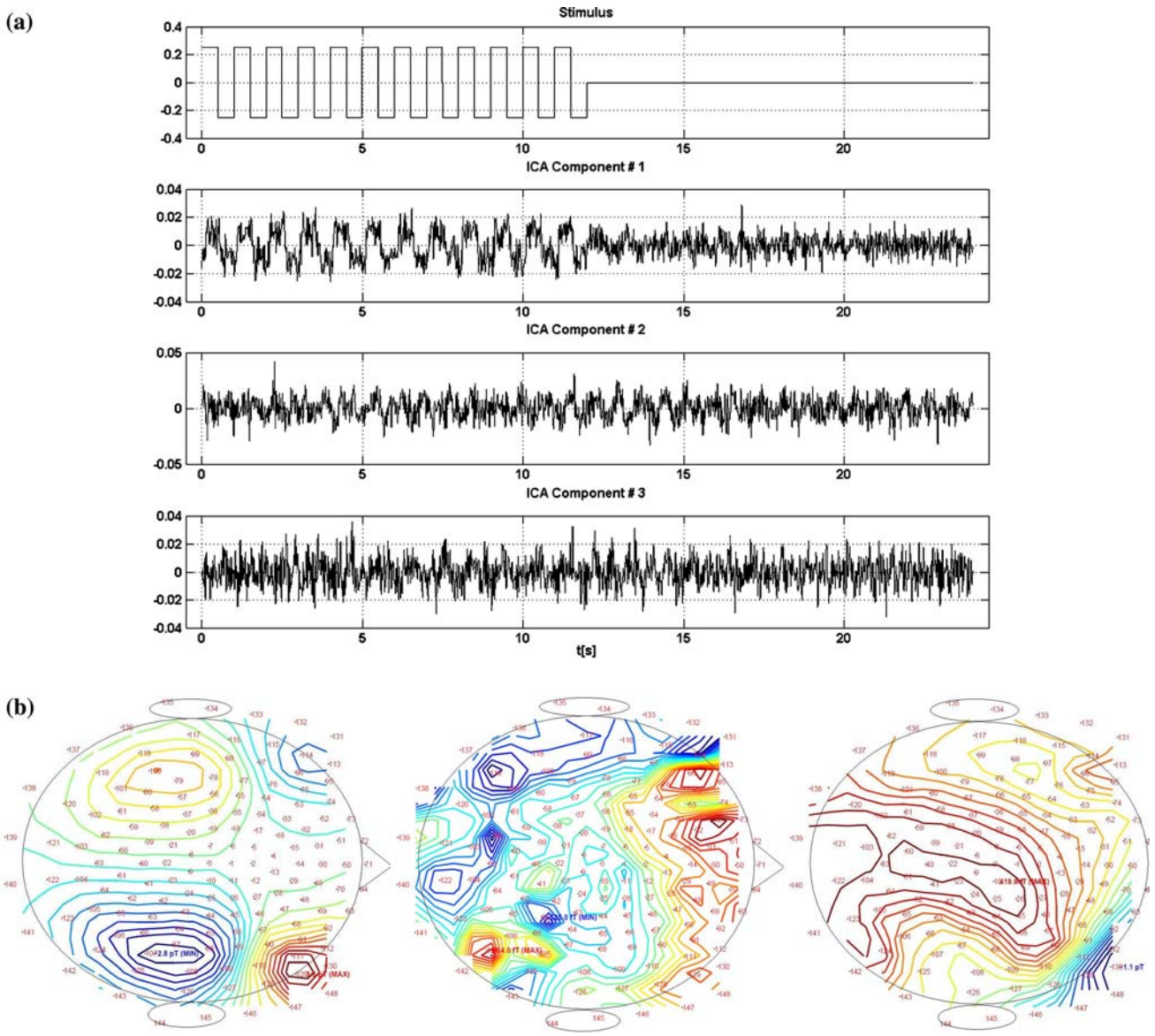

Fig. 4 Spatiotemporal illustration of the main ICA components of the MEG signal of subject #2 in Table 1. (**a**) Stimulus profile and the three most powerful components of the ICA. The first component is correlated with the stimulus and we define it as the "main ICA component" in the text. (**b**) Spatial pattern of the ICA components whose temporal pattern is illustrated in **a**. The left, middle, and right contour maps are related to the first, second, and third ICA components in **a**

in Fig. 4 (first component has the maximum power). As illustrated in Fig. 4a, the first component has the highest temporal correlation with the stimulus profile. In addition, in Fig. 4b, the array of MEG amplitudes of this component is very similar to a contour map of MEG data from two current dipole sources with one in the left and right primary auditory cortices of the subject's brain. In contrast, the spatial patterns of the other two components are primarily composed of noise and cortical activation distant from the primary auditory cortices. Similarly, for each of the other subjects, only one ICA component was well-correlated with a signal from primary auditory cortices. This component is hereafter called "main ICA component".

It should be noted that multiple cortical areas are involved in auditory tasks. However, a simple tone stimulus was chosen for this study because the most prominent activation occurs in the primary auditory area (Salmelin 2007). This is why we were able to extract the primary auditory activation as the strongest single ICA component.

Parameter Estimation

After registering the MEG coordinates to the 3-D anatomical MRI data, the cortical model is constructed consisting of about 2,500 cortical locations in the subject's gray matter. A spherical head model matched to skull

curvature in 6 different brain regions was used to construct the forward model. We use the main ICA component for activation detection in MEG. If one component is considered as the MEG signal in all sensors, the time course of each sensor will be equal to the time course of this component multiplied by a scalar. The spatial pattern of the ICA component is the value of this scalar at all the sensors. The contour map of the spatial pattern of a representative subject is shown in Fig. 4b. We need to solve the MEG inverse problem for this spatial pattern of MEG amplitudes. There are several methods in the literature for solving the inverse problem of EEG/MEG (Baillet et al. 2001). As explained in preprocessing section, we use MEG-Tools to co-register the MEG coordinates to the 3-D MRI data and to construct the cortical model. We use the Multi-Resolution FOCUSS (MR-FOCUSS) (Moran et al. 2005) method, which is implemented in the MEG-Tools, to solve the MEG inverse problem. The MR-FOCUSS is a variant of the standard FOCUSS algorithm (Gorodnitsky and Rao 1997), which has the ability to find both focal and extended sources. The detected activation corresponding to the spatial pattern of Fig. 4b is shown in Fig. 5. As illustrated in Figs. 3 and 5, the fMRI and MEG detected activations have appropriate spatial correlation.

For comparing the spatial responses of fMRI and MEG, detected activations of both techniques are mapped to the Talairach coordinate system (Talairach and Tournoux 1988). The primary auditory cortex in the temporal lobe is expected to be involved in processing of the tone stimulus. Therefore, we restrict the spatial comparison to the activations in the left temporal lobe (LTL) and right temporal lobe (RTL). For each technique, two voxels (one in the LTL and another in the RTL) with maximum activation are selected and then the center of mass of the activations is calculated considering all active voxels whose distances from the maximum voxel are less than 10 mm. Table 2 shows the locations of the activations in the Taliarach coordinate system. As shown in this table, detected activations by both techniques for almost all subjects are located in Brodmann areas 41 and 42, which are the typical areas involved in the initial perception of tone stimuli (Salmelin 2007). In addition, the difference between the spatial responses of fMRI and MEG is small.

Considering the main ICA component, the corresponding MEG signals on the sensors, $B(t)$, can be decomposed into a spatial array of MEG sensor amplitudes, $(b_1 \ldots b_m)^T$, multiplied by the corresponding time sequence of activation, $IC(t)$, (the main ICA component).

$$B(t) = (\, b_1 \quad \ldots \quad b_m \,)^T \cdot IC(t) \tag{5}$$

The inverse solution of Eq. 2 gives $\hat{Q}(t) = G^+ \cdot B(t)$ where G^+ is the inverse kernel of G. Combining the inverse solution, Eq. 2, and Eq. 5, we have:

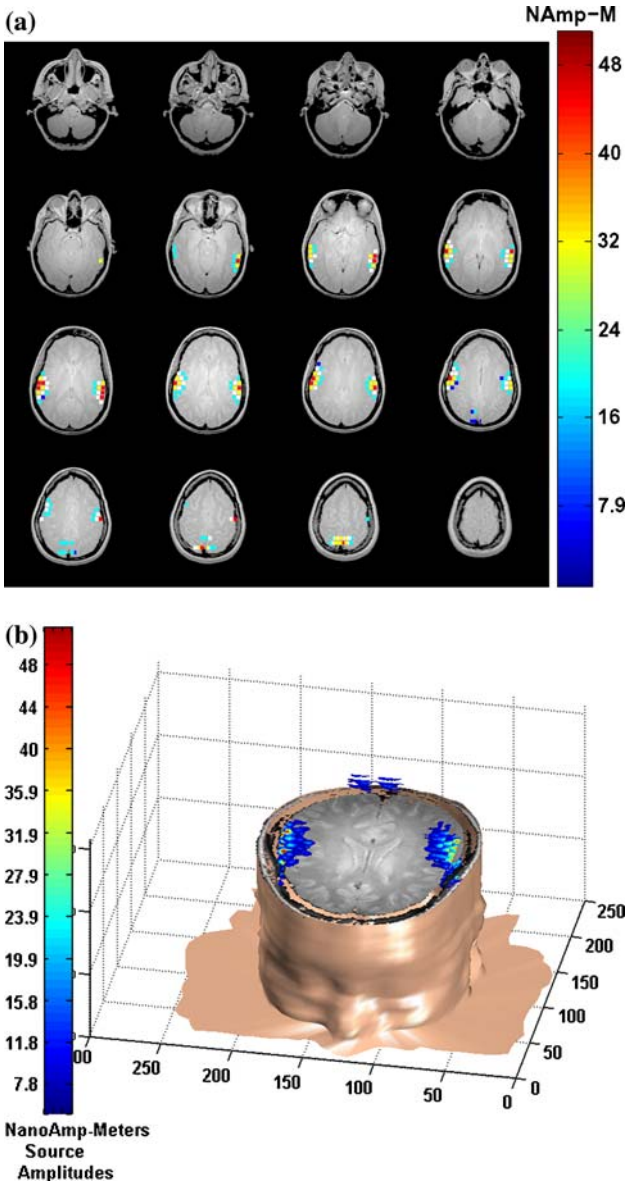

Fig. 5 MEG detected activations of subject #2 after co-registration to the 3-D anatomical MRI data. (**a**) 2-D illustration of the detected activations (axial view). (**b**) 3-D Illustration of the detected activations

$$\hat{Q}(t) = G^+ \cdot (\, b_1 \quad \ldots \quad b_m \,)^T \cdot IC(t) \tag{6}$$

Comparing (1) with (6), it can be assumed that $\hat{N}(t) \propto IC(t)$ and $\hat{K}_M \propto G^+(\, b_1 \quad \ldots \quad b_m \,)^T \cdot G^+(\, b_1 \quad \ldots \quad b_m \,)^T$ shows the spatial pattern of K_M as the estimated amplitudes of the sources. It should be noted that the magnitude of K_M depends on the stimulus paradigm, and the amplitude of this estimated K_M cannot be generalized to other paradigms or other cortical locations.

After calculating $\hat{N}(t)$ from $IC(t)$, it is possible to estimate parameters of the linear filter with the given $\hat{N}(t)$ and the stimulus. For all subjects, we found that a first order linear filter generates reasonable estimation results. Thus, we use the following first order linear filter.

Table 2 Locations of the MEG and fMRI activations mapped to the Taliarach coordinate system

Subject #	Location of activation in right temporal lobe			Location of activation in left temporal lobe		
	Talariach coordinate MEG	Talairach coordinate fMRI	Dist. (mm)	Talariach coordinate MEG	Talairach coordinate fMRI	Dist. (mm)
1	(−62.55, −28.19, 18.08) BA 42	(−46.1, −30.85, 18.24) BA 41	16.66	(48.99, −40.6, 18.16) BA 22	(54.86, −32.27, 16.74) BA 42	10.29
2	(−55.24, −31.23, 19.74) BA 42	(−51.34, −22.35, 16.92) BA 41	10.10	(52.38, −13.51, 21.41) BA 41	(44.56, −13.41, 19.7) BA 42	8.01
3	(−43.96, −25.38, 16.13) BA 41	(−53.29, −39.35, 16.21) BA 22	16.80	(51.15, −35.07, 14.65) BA 22	(52.49, −46.08, 19.58) BA 22	12.14
4	(−57.14, −22.26, 17.74) BA 41	(−45.37, −24.81, 23.76) BA 41	13.46	(60.89, −28.82, 18.71) BA 42	(55.09, −38.96, 18.5) BA 22	11.68
		(−59.15, −32.06, 19.89) BA 42	10.23		(56.27, −46.93, 19.49) BA 22	18.71
5	(−51.19, −47.31, 19.23) BA 22	(−55.24, −31.23, 19.74) BA 42	16.59	(61.58, −37.63, 20.71) BA 22	(55.43, −22.17, 19.78) BA 41	16.66
		(−47.44, −40.19, 21.16) BA 22	8.28		(54.86, −32.27, 16.74) BA 42	9.47
6	(−53.95, −31.3, 19.37) BA 42	(−47.79, −14.46, 21.15) BA 41	18.02	(54.86, −32.27, 16.74) BA 42	(44.56, −13.41, 19.7) BA 41	21.69
7	(−41.27, −11.16, 20.18) BA 41	(−50.13, −23.64, 17.57) BA 41	15.33	(55.55, −26.99, 18.56) BA 42	(46.02, −30.43, 21.91) BA 41	10.67

For each technique, two voxels (one in the left temporal lobe and another in the right temporal lobe) with maximum activation are selected and then the center of mass of the activations is calculated considering all active voxels whose distances from the maximum voxel are less than 10 mm. Locations of the activation in the Taliarach coordinate system (x,y,z) and the corresponding Brodmann Areas (BA) are illustrated in the table

$$T_p \frac{\mathrm{d}N(t)}{\mathrm{d}t} + N(t) = K\ Stm(t - T_d) \tag{7}$$

where T_p, T_d, and K are parameters to be estimated. To calculate $\hat{N}(t)$ from $IC(t)$, we can consider any value for a constant scalar "a" as $\hat{N}(t) = a \cdot IC(t)$. According to (7), the effect of the scalar "a" can be considered in the parameter K and the unit norm $IC(t)$ can be considered as $\hat{N}(t)$. Considering noise, to estimate the parameters of the above linear filter, we have:

$$\begin{cases} N(t;\theta) = h(t;\theta) * \ Stm(t) \\ \hat{N}(t) = N(t;\theta) + e(t) \end{cases} \tag{8}$$

where $e(t)$ models the physiological and instrumental noises, $\hat{N}(t)$ is $IC(t)$ calculated from the main ICA component of the MEG data, and $h(t;\theta)$ is the impulse response of the linear filter in Eq. 7 with parameters $\theta = (T_p, T_d, K)$. Assuming Gaussian noise ($e \sim N(0, \Sigma)$), the parameters can be estimated by the maximum likelihood (ML) method as follows:

$$\begin{aligned} \hat{\theta}_{ML} &= \arg\max_{\theta} f(\hat{N};\theta) \\ &= \arg\min_{\theta}(-\log[f(\hat{N};\theta)]) \\ &= \arg\min_{\theta} \frac{[\hat{N}(t) - N(t;\theta)]^T \Sigma^{-1} [\hat{N}(t) - N(t;\theta)]}{2}. \end{aligned}$$

where $f(.)$ is the probability density function. Finding θ with ML method leads to a weighted least square method with weight matrix Σ. Under the white noise assumption ($\Sigma = \sigma^2 I$), it leads to minimize the following least square function:

$$E(\theta) = \sum_t [\hat{N}(t) - N(t;\theta)]^2. \tag{9}$$

We use the numerical minimization method proposed in (Ljung 1999) for estimating $\theta = (T_p, T_d, K)$ where a quasi-Newton method using values of $E(\theta)$ as well as its gradient is employed. This method is implemented in Matlab (http://www.mathworks.com/). The $N(t)$ and $\hat{N}(t)$ for all subjects are illustrated in Fig. 6. The estimated values of $\theta = (T_p, T_d, K)$ for all subjects are given in Table 3. The signal-to-noise ratio related to the estimation of the linear filter in MEG (SNR_M) in this table is defined as $SNR_M = \|\hat{N}(t)\| / \|\hat{N}(t) - N(t)\|$. It should be noted that SNR_M may rather be considered as a measure of the model fit rather than an SNR. As illustrated in Fig. 6 and values of SNR_M in Table 3, the MEG data of some of the subjects have low SNR_M and thus the standard deviation (STDV) of the estimated parameters are a little high. We were able to slightly increase SNR_M and decrease STDV of the estimated values by using higher order linear filters, but it did not generate much improvement in the variance of the estimated model parameters.

For estimating the parameters related to the fMRI part of the model, we use estimation of $\theta = (T_p\ ,\ T_d\ ,\ K)$ and calculate the estimated $N(t)$ according to (7). The overall

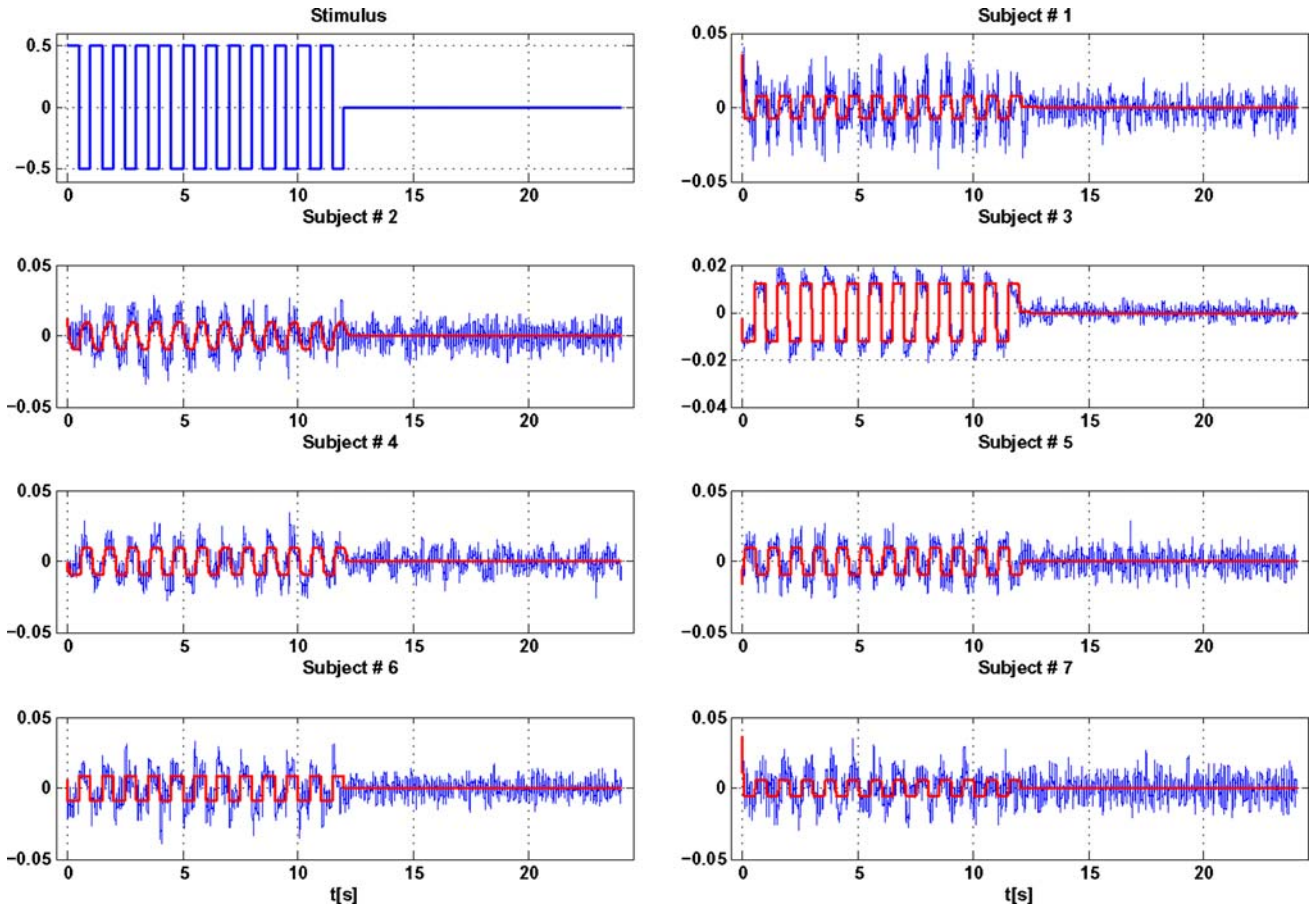

Fig. 6 Illustration of the estimated output of the linear filter in Eq. 7 and real MEG signals. Top-left subplot shows the stimulus as input of Eq. 7. Other subplots show estimated $N(t)$ (red plot) as output of Eq. 7 and real signal (blue plot) as main ICA component from MEG data

synaptic activities $\bar{u}(t)$ is calculated using $N(t)$ according to (3) and then the estimated BOLD response in each active voxel will be generated using $\bar{u}(t)$ and the EBM in (4). According to proportionality of $N(t)$ and $\bar{u}(t)$ in (3) and considering "$\varepsilon\bar{u}(t)$" as input of the EBM in (4), we use normalized $N(t)$ as $\bar{u}(t)$ in (4) and the effect of K_f in (3) is considered in ε.

Parameters of the EBM are estimated by minimizing the error between the estimated and real fMRI signals. The measured BOLD signal can be modeled as follows:

$$y = g(\bar{u};\eta) + e, \quad e \sim N(0,\Sigma) \tag{10}$$

where $g(\bar{u};\eta)$ is the output of the dynamical system of the EBM with input $\bar{u}$ (overall synaptic activities) according to (4), $\eta = (\varepsilon, \tau_s, \tau_f, \tau_0, \alpha, E_0, V_0)$ is physiological parameters of the EBM, and e is the Gaussian measurement noise with variance Σ. If the nonlinear effects of the EBM are small enough, then the effect of physiological noise could be approximated as additive Gaussian noise and e in (10) could model both measurement and physiological noises (Deneux and Faugeras 2006). Using similar steps to derive Eq. 9, the ML estimation of the parameter η leads to the following least square estimation assuming white Gaussian noise ($\Sigma = \sigma^2 I$):

$$\hat{\eta}_{LS} = \arg\min_{\eta} \sum_{t} [g(\bar{u}(t);\eta) - y(t)]^2 \tag{11}$$

As described in preprocessing section, the active voxels for each subject are chosen, and their mean BOLD signal over all blocks is calculated and assumed as $y(t)$ in (11). Then, parameters of the EBM are estimated using a numerical minimization method. A basic question about the identifiability of the EBM in (4) is that if we know the system input $\bar{u}$ and output y, do we have enough information to determine unique values for the parameters? In general, there is no unique solution for the parameter estimation of the EBM in (4) because the effects of some parameters on the output do interfere with those of others (Deneux and Faugeras 2006). For example, when the input of the EBM is low enough to make the linear approximation of the model, two parameters ε and V_0 as the scale factor on the input (ε) and that on the output (V_0) have interfering effects. In fact, increasing ε could be compensated by decreasing V_0 by the same factor to

Table 3 Estimated values of the parameters of the proposed integrated model using real auditory data of 7 normal subjects

Subject #	Parameters of the linear filter in (7)				Parameters related to the extended balloon model in fMRI						
	K	T_p (ms)	T_d (ms)	SNR_M	Number of active voxels	σ (mm)	ε	τ_s (S)	τ_f (S)	τ_0 (S)	SNR_f
1	0.016	20	74	0.87	40	10.06	0.21 (0.14)	2.30 (0.67)	1.84 (0.73)	1.49 (0.50)	4.16
2	0.020	100	0	0.98	10	5.55	0.17 (0.13)	2.04 (1.91)	2.75 (0.75)	1.44 (0.43)	1.81
3	0.025	14	1	3.20	21	10.67	0.13 (0.12)	1.05 (0.83)	3.93 (1.78)	2.30 (1.10)	3.25
4	0.019	44	59	1.23	42	7.87	0.17 (0.15)	1.40 (1.11)	3.65 (1.53)	2.70 (1.20)	3.15
					28	10.11	0.16 (0.14)	1.40 (0.63)	4.23 (1.82)	2.30 (0.85)	3.54
5	0.020	31	72	1.40	82	8.01	0.17 (0.17)	1.93 (1.36)	3.44 (1.64)	2.82 (1.08)	3.03
					67	11.29	0.16 (0.14)	1.75 (0.89)	3.77 (1.65)	2.85 (0.96)	2.50
6	0.017	3	0	1.08	56	11.51	0.34 (0.32)	1.35 (0.51)	2.27 (0.88)	1.63 (0.64)	9.39
7	0.012	20	39	0.63	44	16.86	0.26 (0.17)	2.16 (0.88)	3.26 (1.16)	1.68 (0.79)	6.51
Mean	0.018	33	35	–	–	10.21	0.20	1.74	3.23	2.27	–
STDV	0.004	32	34			3.15	0.19	1.04	1.58	1.07	

The parameter T_p, T_d, and K are related to the linear filter in Eq. 7. Values under columns ε, τ_s, τ_f, and τ_0 are the mean value and the standard deviation (values in parentheses) of these estimated parameters from all active voxels of the corresponding subjects. Mean and STDV rows show the average and the standard deviation of the estimated parameters for all subjects, respectively. $\alpha = 0.33$, $E_0 = 0.34$, and $V_0 = 0.03$ ($V_0 = 0.06$ for subject #6) were fixed at their physiological mean values. MEG linear filter signal to noise ratio (SNR_M) is defined as $SNR_M = \|\hat{N}(t)\|/\|\hat{N}(t) - N(t)\|$ where $\hat{N}(t)$ is the estimate of $N(t)$ according to (7). fMRI Signal to noise ratio (SNR_f) is defined as $SNR_f = \|\hat{y}(t)\|/\|\hat{y}(t) - y(t)\|$ where $\hat{y}(t)$ and $y(t)$ are estimated and real BOLD signals, respectively

produce exactly the same output. It would not be possible to estimate these two parameters. Rather, only their product can be estimated.

For reducing the redundancy, we fix $\alpha = 0.33$, $E_0 = 0.34$, and $V_0 = 0.03$ ($V_0 = 0.06$ for subject #6) at their physiological mean values according to (Friston et al. 2000) and estimate the remaining parameters $\eta = (\varepsilon, \tau_s, \tau_f, \tau_0)$. The optimization procedure for estimating the parameters of the EBM using the BOLD signal is shown in Fig. 7. The sum square error in (11) is the objective function whose minimization gives the optimal values of the unknown parameters. The Nelder–Mead simplex search method is used as the principal algorithm for unconstrained minimization (Lagarias et al. 1998). Before starting to estimate unknown parameters $\eta = (\varepsilon, \tau_s, \tau_f, \tau_0)$, the parameters of the linear filter in Eq. 7 are estimated using the MEG data and the estimated $N(t)$ is considered as the overall synaptic activity ($\bar{u}(t)$ in Eq. 4) as shown in Fig. 7. The iterative optimization process is started by choosing proper initial values for the unknown parameters. The parameters are updated by minimizing the sum square error between the given BOLD signal and the estimated BOLD signal using the values of the parameters in the previous step. We implement the Nelder–Mead simplex search method by the "*fminsearch*" function in Matlab. "*Simulink*" is used to solve the nonlinear state-space Eq. 4 by the iterations of the "*fminsearch*" minimization.

The estimated parameters of the EBM for all subjects are given in Table 3. For each subject, the value of the parameter in this table is the mean of the estimated parameter in all active voxels. The histograms of 4 estimated parameters of the EBM for all subjects are illustrated in Fig. 8. We use principal component analysis (PCA) to extract the main component of the BOLD signal from all active voxels in each subject. Then, we estimate parameters of the EBM for this component. The estimated and the real BOLD signals for this PCA component of all subjects are shown in Fig. 9.

For reducing the redundancy of the parameters of the EBM, we consider fixed values for three parameters (α, E_0, and V_0) and estimate the remaining four parameters (ε, τ_s, τ_f, τ_0). Considering the fixed values ($\alpha = 0.33$, $E_0 = 0.34$, and $V_0 = 0.03$), the optimization procedure shown in Fig. 7 is successfully executed for all subjects except Subject #6. This subject has strongest BOLD signal compared to others as shown in Fig. 9. According to the linear relationship between the BOLD signal and V_0 in (4), a larger value for V_0 is expected for this subject compared to others. When $V_0 = 0.03$ is fixed for this subject, the optimization procedure becomes unstable and the value of ε tends to be very large to compensate the assumed small value of V_0. Stable optimization needs larger values for V_0. A stable optimization for this subject is obtained by considering $V_0 = 0.06$. However, value of ε is still large for this subject as shown in Table 3. Subject #7 also has high BOLD contrast and its estimated ε has a large value. Large variation of ε shown in Fig. 8 is related to the fact that we assign a fixed value to V_0 and compensate its possible variation by ε.

The BOLD contrast of some subjects has low SNR as shown in Fig. 9 and Table 3. There are outliers in their real

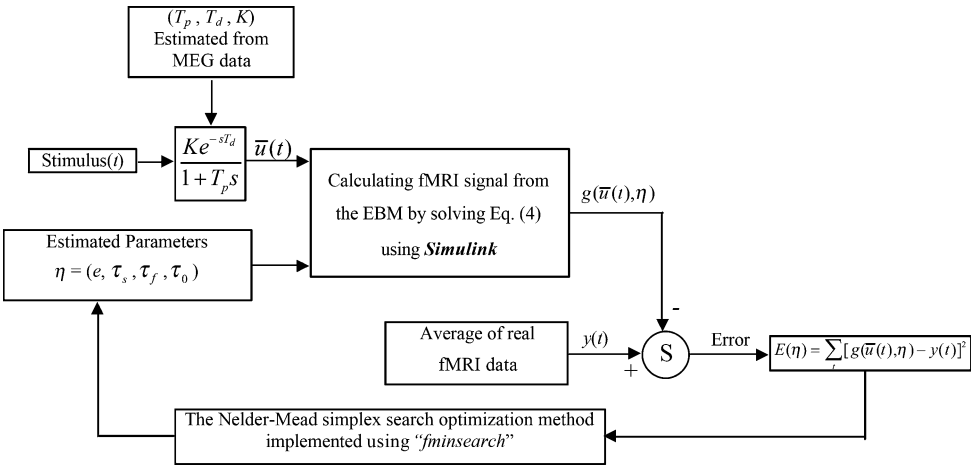

Fig. 7 Illustration of the optimization procedure for estimating the parameters of the EBM using the BOLD signal. The parameters of the linear filter in Eq. 7 are estimated using MEG data and the output $N(t)$ is given as $\bar{u}(t)$ in Eq. 4. The Nelder–Mead simplex search optimization method is implemented using the "*fminsearch*" function in Matlab (Lagarias et al. 1998). The "*fminsearch*" function minimizes the sum square error between the real and estimated BOLD signals by iteratively changing the parameters of the EBM. "*Simulink*" is used to solve the nonlinear state-space Eq. 4

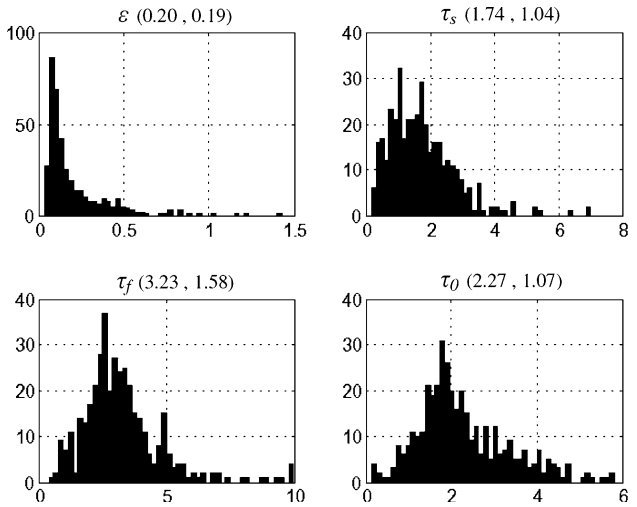

Fig. 8 Histograms of the estimated parameters (ε, τ_s, τ_f, τ_0) of the EBM for all subjects. $\alpha = 0.33$, $E_0 = 0.34$, and $V_0 = 0.03$ ($V_0 = 0.06$ for subject #6) were fixed at their physiological mean values. Left and right values in parentheses of each subplot show the mean and the standard deviation of the estimated parameters, respectively

fMRI data. As "*fminsearch*" may find any minimum of Eq. 11, outliers can cause finding a local minimum instead of the global minimum. However, using l1 norm instead of l2 norm in (11) can reduce the effect of outliers. Thus, we repeat the estimation of the parameters using l1 norm. However, mean values of the estimated parameters of the active voxels do not change significantly compared to the results from l2 norm given in Table 3. The Nelder–Mead simplex search optimization method (Lagarias et al. 1998) is used for the implementation of the optimization using both l1 and l2 norms.

The estimated values of the parameters of the EBM shown in Table 3 are in agreement with other works (Deneux and Faugeras 2006; Friston et al. 2000). Reasonable mean and STDV of the estimation are due to the fact that all datasets are from the normal subjects with the same stimulus. In addition, we have two series of fMRI datasets for subjects #4 and #5 whose estimated parameters are similar as shown in Table 3. High inter-subject variability of the MEG parameters (T_p and T_d) in Table 3 is related to low SNR of the MEG signal. Although these parameters are further used to calculate the input of the EBM for estimating its parameters, delays in the order of 10 ms in the input of the EBM cause very little change in output due to the slow behavior of the EBM. Finally, Figs. 6 and 9 illustrate goodness of fit of the real MEG and fMRI datasets to the proposed integrated MEG/fMRI model.

As the final stage, we estimate the parameter related to the spatial crosstalk in fMRI. Figure 3 illustrates the detected activation from the fMRI time series of subject #2 after removing the single active voxels. For estimating the spatial crosstalk represented by $\sigma = (\sigma_x, \sigma_y, \sigma_z)$ in Eq. 2 in (Babajani et al. 2005), two Gaussian kernels are fitted to the main clusters of the detected activation areas in left and right primary auditory cortices. We assume an isotropic Gaussian kernel with $\sigma_x = \sigma_y = \sigma_z$ for estimating σ_x, σ_y, and σ_z. The hotspot of the cluster is assumed as the center of the Gaussian kernel. All neighboring voxels to the central voxel in a sphere with a diameter of 25 mm are considered for curve fitting. The estimated σ is given in Table 3.

In this study, we propose a method to estimate the parameters of the integrated MEG/fMRI model using real auditory stimulus. However, the proposed estimation

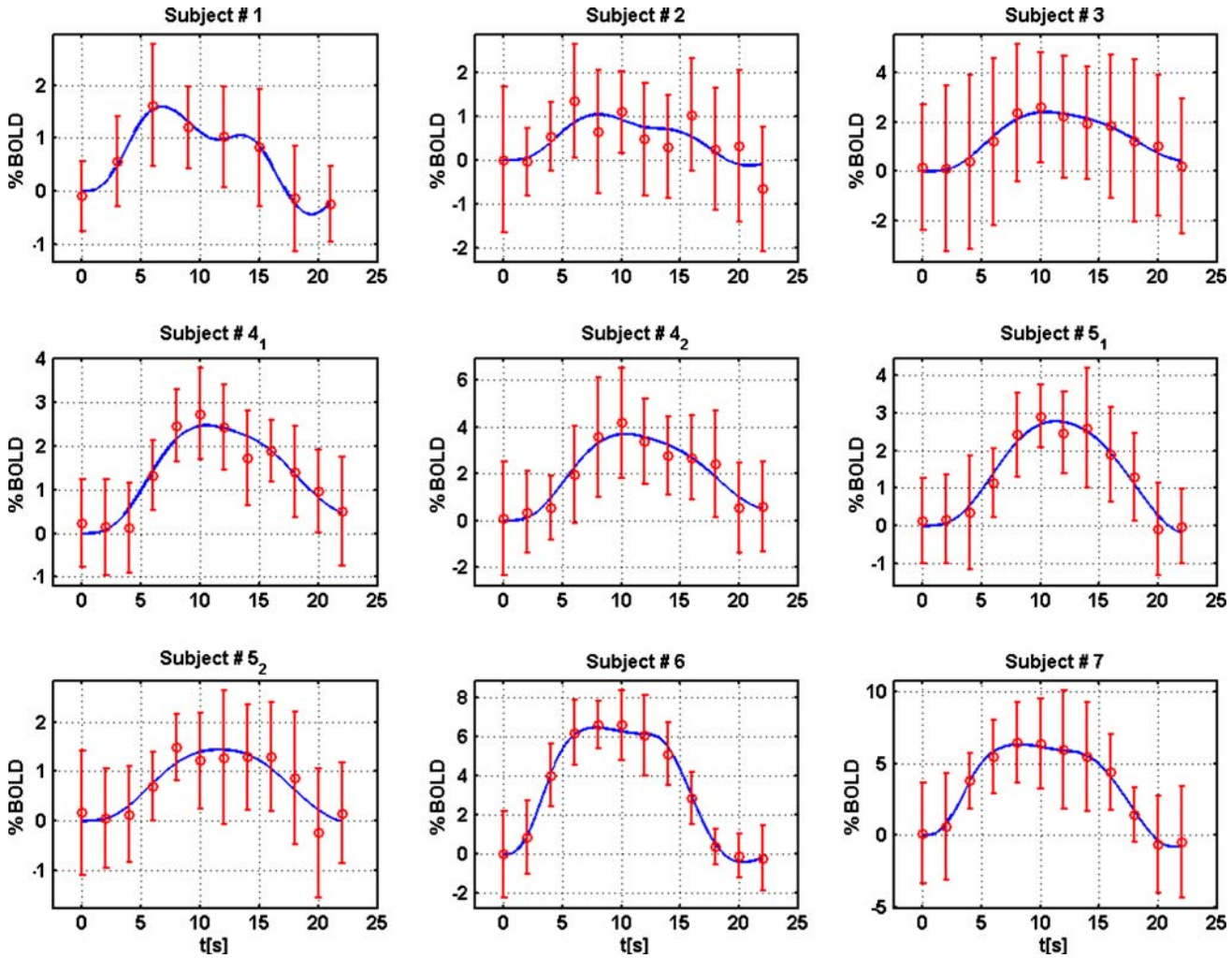

Fig. 9 Illustration of the real and the estimated BOLD signals. Red plots show the PCA main component extracted from the real data of all active voxels in each subject. This PCA component is the average of all blocks; o-plot and error-bar show the mean and the STDV of BOLD signals, respectively. The estimated BOLD signals are illustrated by blue lines. 2 series of fMRI data for subjects #4 and #5 were used as specified by subscripts 1 and 2 in title of the corresponding subplots

procedure can be used for other types of stimulus. The parameters of the model have different levels of dependency on the stimulus. Parameter K_M as the spatial pattern of activation has strong dependency on the type of stimulus. For example, we expect different spatial responses (different K_M) for a visual stimulus compared to an auditory stimulus. Parameters of the linear filter (7) have variations that, depending on the strength and type of the stimulus. K in (7), may change over a wide range due to the variation of the strength of the stimulus. But, T_p, the time delay between the stimulus onset and the maximum MEG activation, may exhibit less variation for different stimulus types. Although hemodynamic parameters (ε, τ_s, τ_f, τ_0, α, E_0, V_0) may change for different stimulus types and strengths, their variations are limited based on the physiology (Friston et al. 2000).

The proposed model with the parameters estimated from the real data can be used in simulating realistic datasets for comparing different integrated EEG/MEG and fMRI analysis methods. After estimating parameters of the model using real EEG/MEG and fMRI datasets for a particular stimulus, generating EEG/MEG and fMRI signals for this stimulus is straightforward. The estimated K_M (as the spatial pattern of the MEG activation), $N(t)$, and G will be used to generate the simulated EEG or MEG signals based on Eq. 2. $N(t)$ as the number of active PSPs at time point t will be calculated using Eq. 7 and the given stimulus profile. Solution of the forward problem will generate the lead field matrix G. To generate the simulated BOLD signal, Eq. 4 will be used with the calculated $N(t)$ and the estimated parameters of the EBM (ε,τ_s, τ_f, τ_0, α, E_0, V_0). Different values of SNR for both EEG/MEG and fMRI

signals can be generated by adding the additive noise in neuronal level ($N(t)$) as well as in the measurements as shown in Fig. 1.

Discussion

The relationship between strength of stimulus and the generated neural activity in the cortical areas should be generally nonlinear. This nonlinearity minimally stems from the physiological principle that the strength of stimulus can be theoretically unlimited but the number of neurons and their synapses are limited. However, this relationship within a certain range of change in stimulus strength has been reported to be linear (Arthurs et al. 2007). In addition, this nonlinear relationship can be locally approximated by a linear relationship using the Taylor series expansion when the strength of the stimulus changes within a small range.

PSPs and action potentials (APs) are two indices of neural activity. Although MEG and EEG signals seem to be largely due to the synaptic current flow (Baillet et al. 2001; Hämäläinen et al. 1993), currents related to APs may contribute to the MEG and EEG signals (Curio et al. 1994; Hashimoto et al. 1996). In (Babajani et al. 2005), we assumed that the PSPs are the main source of the neural activity and generate the MEG and EEG signals. After the stimulus onset, the number of fired PSPs and consequently the number of active neurons in the active cortical areas will gradually increase. In an active area, we model the mean number of the fired PSPs by a simple first order linear filter according to Eq. 7. $N(t)$ in Eqs. 1 and 7 represents the mean number of the fired PSPs at time point t in the desired active area.

To model $N(t)$ in a large range of stimulus strength, a nonlinear model should be used. However, we use a special case (fixed strength of an auditory stimulus) in this study where a linear model can be extracted. As indicated in section of "Parameter Estimation," we have tried to improve the approximation of the dynamics of the linear filter using higher order linear filters, although it did not generate much improvement in the results. For a stimulus that involves multiple cortical areas with interactions between the areas, we expect more complex dynamics. In this study, we use the simple auditory stimulus, which involves limited areas (mostly the primary auditory cortices) and thus the simple first order filter seems to be sufficient to characterize the dynamics of the model.

Referring to Eqs. 8–13 in (Babajani et al. 2005), the sum of the PSPs' activities generates a current dipole whose projected amplitude on the direction perpendicular to the cortical surface is:

$$Q(t) = \int_{\tau} \left(\sum_{k=1}^{N(t-\tau)} w_k \beta_k \Delta V_k \varphi_k(\tau) \cos(\theta_k) \right) .\mathrm{d}\tau \tag{12}$$

where subscript k shows the kth fired synapse, $N(t)$ is the number of fired PSPs at time point t, value of w_k is +1 for excitatory PSP (EPSP) and -1 for inhibitory PSP (IPSP), ΔV_k shows the peak value of the kth PSP, β_k models parameters of the kth synapse and its neighboring dendrites, φ_k (t) is normalized waveform of the kth PSP, and $\cos(\theta_k)$ shows projection of amplitude of the kth current dipole on the direction perpendicular to the cortical surface. The following normalized waveform φ_k (t) was proposed in (Babajani et al. 2005) and is based on previous studies (Almeida and Stetter 2002; Larkum et al. 1998):

$$\varphi_k(t) = \frac{t e^{-\frac{(t-\tau_k)}{\tau_k}}}{\tau_k} \tag{13}$$

where τ_k is the time constant of φ_k (t).

We introduced appropriate probability distribution functions (pdfs) for the random variables w_k, ΔV_k, β_k, θ_k, and τ_k (Babajani et al. 2005). Considering the mean values of these variables, the mean value of $Q(t)$ in Eq. 12 can be calculated as follows (see Section III in (Babajani et al. 2005) for more explanations):

$$\overline{Q}(t) = \bar{V}\,\bar{\beta}\,\left((1-r(t))\cdot\ g(\sigma_T^E)\ -\ r(t)\ g(\sigma_T^I)\ \right) \cdot \int_{\tau} \overline{\varphi}(\tau) \sum_{k=1}^{N(t-\tau)} \mathrm{d}\tau \tag{14}$$

where $\overline{\varphi}(\cdot)$ is the mean of φ_k (t), $\overline{V}$ is the mean of ΔV_k, $\overline{\beta}$ is the mean of β_k, $r(t)$ is the ratio of the number of active IPSPs to the number of all active PSPs, and $g(\sigma_T^E)$ and $g(\sigma_T^I)$ are related to the spatial distributions of the EPSPs and IPSPs, respectively. Although $r(t)$ may change after stimulus onset, its variation is small in the current study because we use a specific type and fixed strength of an auditory stimulus and thus $r(t)$ can be approximated by a time-invariant coefficient r. Considering the effects of all time-invariant coefficients of Eq. 14 in K, Eq. 14 can be written as:

$$\overline{Q}(t) = K \cdot \int_{\tau} \overline{\varphi}(\tau) \cdot N(t-\tau)\mathrm{d}\tau = K \cdot \overline{\varphi}(t) * N(t) \tag{15}$$

where "*" is the convolution operator. Considering the step response in Eq. 7, the Laplace transform of Eq. 15 is as follows:

$$\overline{Q}(S) \propto \Phi(S) \cdot N(S) \propto \left(\frac{1}{(S+\frac{1}{\tau})^2} \right) \cdot \left(\frac{e^{-T_d \cdot S}}{S(S+\frac{1}{T_P})} \right) \tag{16}$$

where $\Phi(S)$ and $N(S)$ are Laplace transforms of $\overline{\varphi}(t)$ and $N(t)$, respectively; τ is the mean of τ_k based on Eq. 13

whose value is 2.8 ms referring to its pdf in (Babajani et al. 2005), and T_p and T_d are the parameters of the linear filter in Eq. 7. Referring to Table 3, the mean value of the estimated T_p is 33 ms. Poles of $N(S)$ are zero and $-1/T_P = -30.3$ Hz. Pole of $\Phi(S)$ is $-1/\tau = -357.1$ Hz. The dominant poles of $\overline{Q}(S)$ are poles of $N(S)$, and thus we can neglect the effect of $\Phi(S)$ on $\overline{Q}(S)$. Therefore, we can conclude that $\overline{Q}(S) \propto N(S)$ or $\overline{Q}(t) \propto N(t)$; we use this fact in Eq. 1.

The relationship between the stimulus and the generated BOLD signal can be separated into three steps: a step from the stimulus to the neural activity, another step from the neural activity to the CBF and a final step from the CBF to the BOLD signal. The step from the CBF to the BOLD signal was described by the proposed nonlinear Balloon model (Buxton et al. 1998). For the step from the neural activity to the CBF, Friston et al. proposed a model of CBF autoregulation and added this relationship to the model of Buxton et al. in the extended Balloon model (Friston et al. 2000). They used the waveform of the stimulus as the neural activity while the relationship between the stimulus and the neural activity should be nonlinear as reported in some experimental studies (Jones et al. 2004; Nielsen and Lauritzen 2001).

As mentioned before, the linear relationship between the stimulus and the neural activity is an acceptable approximation in the case of this study where we used stimulus of fixed strength. To derive the neural activity as the input of the EBM, we assumed that the neural activity is proportional to the synaptic activity (Babajani et al. 2005), which was defined as the total consumed energies by the PSPs. In addition, we considered the same rule for both EPSPs and IPSPs to calculate the synaptic activity. This assumption was based on experimental studies (Caesar et al. 2003). Finally, we concluded that the synaptic activity was linearly related to $N(t)$ (see Eqs. 5–7 and 19 in Babajani et al. 2005). Out first assumption about the proportionality of the neural activity to the consumed energy of the PSPs seems to be acceptable as indicated in other studies (Attwell and Iadecola 2002; Sotero and Trujillo-Barreto 2008).

Conclusion

In this paper, we estimate the parameters of the integrated MEG/fMRI model (Fig. 1) proposed in our previous work (Babajani et al. 2005) using real data. In this model, the external stimulus generates neural activities related to the PSPs which are the common link between MEG and fMRI. We use a first order linear filter to calculate the number of active PSPs as a function of the external stimulus. We summarize the relationship between the number of active PSPs as an index of neural activity that generates the MEG signal. Moreover, we define the relationship between the number of active PSPs and the overall synaptic activity as input of the EBM for generating the fMRI signal. We estimate parameters of the proposed integrated model using real auditory data from 7 normal subjects. We start with an ICA analysis of the MEG signal and show that the main ICA component can be assumed as the number of active PSPs. Parameters of the first order linear filter and parameters of the EBM are estimated using the real data. The proposed model with the parameters estimated from the real data can be used in simulating realistic datasets for comparing different integrated EEG/MEG and fMRI analysis methods.

Acknowledgements The authors thank Mostafa Ghannad-Rezaie for his help with the fMRI and MEG experiments as well as useful discussions. The authors would greatly appreciate Dr. Micah Murray as well as reviewers of the paper for their useful comments. This work was supported by grants from the University of Tehran, Tehran, Iran, and National Institutes of Health (NIH grant R01EB002450), United States and also supported by NIH/NINDS Grant R01-NS30914.

References

Almeida R, Stetter M. Modeling the link between functional imaging and neuronal activity: synaptic metabolic demand and spike rates. Neuroimage. 2002;17:1065–79.

Arthurs OJ, Donovan T, Spiegelhalter DJ, Pickard JD, Boniface SJ. Intracortically distributed neurovascular coupling relationships within and between human somatosensory cortices. Cerebral Cortex. 2007;17(3):661–8.

Attwell D, Iadecola C. The neural basis of functional brain imaging signals. Trends Neurosci. 2002;25:621–5.

Babajani A, Nekooei MH, Soltanian-Zadeh H. Integrated MEG and fMRI model: synthesis and analysis. Brain Topogr. 2005;18(2): 101–13.

Babajani A, Soltanian-Zadeh H. Integrated MEG/EEG and fMRI model based on neural masses. IEEE Trans Biomed Eng. 2006;53(9):1794–1801.

Baillet S, Mosher JC, Leahy RM. Electromagnetic brain mapping. IEEE Signal Proc Mag. 2001;18:14–30.

Buxton RB, Wong EC, Frank LR. Dynamics of blood flow and oxygenation changes during brain activation: the balloon mode. Magn Reson Med. 1998;39:855–64.

Caesar K, Gold L, Lauritzen M. Context sensitivity of activity dependent increases in cerebral blood flow. Proc Nal Acad Sci USA. 2003;100:4239–44.

Curio G, Mackert B, Burghoff M, Koetiz R, Abraham-Fuchs K, Harer W. Localization of evoked neuromagnetic 600 Hz activity in the cerebral somatosensory system. Electroenceph Clin Neurophysiol. 1994;91:483–7.

Dale AM, Halgren E. Spatiotemporal mapping of brain activity by integration of multiple imaging modalities. Curr Opin Neurobiol. 2001;11:202–8.

Dale AM, Liu AK, Fischl BR. Dynamic statistical parametric mapping: combining fMRI and MEG for high-resolution imaging of cortical activity. Neuron 2000;26:55–67.

Daunizeau J, Grova C, Marrelec G, Mattout J, Jbabdi S, Pélégrini-Issac M, Lina JM, Benali H. Symmetrical event-related EEG/fMRI information fusion in a variational Bayesian framework. Neuroimage. 2007;36(1):69–87.

Deneux T, Faugeras O. Using nonlinear models in fMRI data analysis: model selection and activation detection. Neuroimage. 2006;32:1669–89.

Friston KJ, Mechelli A, Turner R, Price CJ. Nonlinear responses in fMRI: the Balloon model, Volterra kernels, and other hemodynamics. Neuroimage. 2000;12:466–77.

Gorodnitsky IF, Rao BD. Sparse signal reconstruction from limited data using FOCUSS: a re-weighted minimum norm algorithm. IEEE Trans Sig Proc. 1997;45(3):600–16.

Hashimoto I, Mashiko T, Imada T. Somatic evoked high-frequency magnetic oscillations reflect activity of inhibitory interneurons in the human somatosensory cortex. Electroenceph Clin Neurophysiol. 1996;100:189–203.

Hämäläinen M, Hari R, Ilmoniemi RJ, Knuutila J, Lounasmaa OV. Magnetoencephalography—theory, instrumentation and applications to noninvasive studies of the working human brain. Rev Modern Phys. 1993;65:413–97.

Horwitz B, Poeppel D. How can EEG/MEG and fMRI/PET data be combined? Hum Brain Mapp. 2002;17:1–3.

Jones M, Hewson-Stoate N, Martindale J, Redgrave P., Mayhew J. Nonlinear coupling of neural activity and CBF in rodent barrel cortex. Neuroimage. 2004;22:956–65.

Korvenoja A, Aronen HJ, Ilmoniemi RJ. Functional MRI as a constraint in multi-dipole models of MEG data. Int J Bioelectrom. 2001;3(1).

Lagarias JC, Reeds JA, Wright MH, Wright PE. Convergence properties of the Nelder–Mead simplex method in low dimensions. SIAM J Optim. 1998;9(1):112–47.

Larkum ME, Launey T, Dityatev A, Luscher HR. Integration of excitatory postsynaptic potentials in dendrites of motoneurons of rat spinal cord slice cultures. J Neurophysiol. 1998;80:924–35.

Liu AK, Belliveau JW, Dale AM. Spatiotemporal imaging of human brain activity using functional MRI constrained magnetoencephalography data: Monte-Carlo simulations. Proc Natl Acad Sci USA. 1998;95:8945–50.

Liu Z, Ding L, He B. Integration of EEG/MEG with MRI and fMRI. IEEE Med Biol Mag. 2006;25(4):46–53.

Ljung L. System identification: theory for the user. USA: Prentice-Hal PTR; 1999.

Martinez-Montes E, Valdes-Sosa PA, Miwakeichi F, Goldman RI, Cohen MS. Concurrent EEG/fMRI analysis by multiway partial least squares. NeuroImage. 2004;22:1023–34.

Moran JE, Bowyer SM, Tepley N. Multi-resolution FOCUSS source imaging of MEG data. Third International Symposium on Noninvasive Functional Source Imaging within the Human Brain and Heart. Biomedizinische Technik. 2001;46:112–4.

Moran JE, Bowyer SM, Tepley N. Multi-resolution FOCUSS: a source imaging technique applied to MEG data. Brain Topogr. 2005;18:1–17.

Moran JE, Drake CL, Tepley N. ICA methods for MEG imaging. Neurol Clin Neurophysiol. 2004;72.

Nielsen AN, Lauritzen M. Coupling and uncoupling of activity-dependent increases of neuronal activity and blood flow in rat somatosensory cortex. J Physiol. 2001;533:773–85.

Nunez PL, Silberstein RB. On the relationship of synaptic activity to macroscopic measurements: does co-registration of EEG with fMRI make sense? Brain Topogr. 2000;13:79–96.

Riera JJ, Aubert E, Iwata K, Kawashima R, Wan X, Ozaki T. Fusing EEG and fMRI based on a bottom-up model: inferring activation and effective connectivity in neural masses. Philos Trans: Biol Sci. 2005;360(1457):1025–41.

Riera JJ, Wan X, Jimenez JC, Kawashima R. Nonlinear local electrovascular coupling. I: a theoretical model. Hum Brain Mapp. 2006;27(6):896–914.

Riera JJ, Jimenez JC, Wan X, Kawashima R, Ozaki T. Nonlinear local electrovascular coupling. II: from data to neuronal masses. Hum Brain Mapp. 2007;28(4):335–54.

Salmelin R. Clinical neurophysiology of language: the MEG approach. Clin Neurophysiol. 2007;118(2):237–54.

Sotero RC, Trujillo-Barreto NJ. Biophysical model for integrating neuronal activity, EEG, fMRI and metabolism. Neuroimage. 2008;39(1):290–309.

Talairach J, Tournoux P. Co-planar stereotaxic atlas of the human brain: 3-Dimensional proportional system-an approach to cerebral imaging. New York: Thieme Medical Publishers; 1988.

Talavage TM, Sereno MI, Melcher JR, Ledden PJ, Rosen BR, Dale AM. Tonotopic organization in human auditory cortex revealed by progressions of frequency sensitivity. J Neurophysiol. 2004;91(3):1282–96.

Tong L, Liu R, Soon VC, Huang YF. Indeterminacy and identifiability of blind identification. IEEE Trans Circuits Syst. 1991;38(5):499–509.